Energy Storage and Conversion 2026, 4(2), 4186.
doi: https://doi.org/10.59400/esc4186

Article

Modeling and optimization of a grid-connected PV–wind–fuel cell hybrid system with hydrogen storage

Youssef El Baqqal*, Mohammed Ferfra, Souleymane Kientega

Department of Electrical Engineering, Mohammadia School of Engineers, Mohammed V University, Rabat B.P. 765, Morocco

*** Corresponding author:** Youssef El Baqqal, Youssef.elbaqqal@um5r.ac.ma

CITATION

El Baqqal Y, Ferfra M, Kientega S. Modeling and optimization of a grid-connected PV–wind–fuel cell hybrid system with hydrogen storage. Energy Storage and Conversion. 2026; 4(2): 4186. https://doi.org/10.59400/esc4186

ARTICLE INFO

Received: 24 March 2026
Revised: 18 April 2026
Accepted: 27 April 2026
Available online: 22 May 2026

COPYRIGHT

Copyright © 2026 Author(s). *Energy Storage and Conversion* is published by Academic Publishing Pte. Ltd. This work is licensed under the Creative Commons Attribution (CC BY) license. https://creativecommons.org/licenses/by/4.0/

Abstract: This paper presents a comprehensive techno-economic and environmental assessment of a grid-connected hybrid renewable energy system (HRES) integrating photovoltaic (PV), wind turbine (WT), and fuel cell (FC) technologies for a case study in Dakhla, Morocco. A detailed modeling framework is developed, including renewable generation, electrolyzer operation, hydrogen storage, and fuel cell conversion, combined with an energy management strategy to coordinate power flows between system components and the utility grid. The system design is formulated as a constrained optimization problem aiming to minimize the total annual cost while incorporating reliability and grid stability requirements through a penalty-based approach. The optimization is performed using a particle swarm optimization (PSO) algorithm to evaluate three system configurations: PV–WT–FC, WT–FC, and PV–FC. The results show that the PV–WT–FC configuration provides the best overall performance, achieving a total annual cost of 186,957 USD, a levelized cost of energy (LCOE) of 0.1472 USD/kWh, and a high renewable energy fraction (REF) of 88.32%. This configuration also ensures excellent reliability (LPSP = 0%) and stable grid operation. In contrast, the WT–FC configuration achieves a lower LCOE of 0.1164 USD/kWh when considering component costs alone; however, it results in significant grid instability, leading to a high penalty cost of 700,588 USD and reduced overall feasibility. Similarly, the PV–FC configuration shows a higher total annual cost (255,425 USD) and lower renewable penetration (60%), making it less competitive. These findings highlight the importance of integrating grid stability and reliability constraints within the optimization framework. The proposed approach effectively identifies balanced system configurations that ensure cost efficiency, high renewable penetration, and stable operation, confirming the robustness and practical applicability of the PV–WT–FC system for sustainable energy deployment.

Keywords: hybrid renewable energy system; hydrogen storage; grid-connected system; particle swarm optimization; energy management; techno-economic analysis; grid stability

1. Introduction

The rapid growth in global energy demand, driven by urbanization and industrial development, has intensified environmental concerns due to the continued reliance on fossil fuels [1]. In response, renewable energy sources such as solar and wind have emerged as sustainable alternatives for reducing greenhouse gas emissions and ensuring long-term energy security. However, the inherent intermittency and stochastic nature of these resources pose significant challenges to maintaining a reliable and stable power

supply [2].

To address these limitations, hybrid renewable energy systems (HRES), which combine multiple energy sources with energy storage technologies, have been widely proposed as effective solutions for improving system reliability and enhancing renewable energy utilization [1,3,4].

Among available storage technologies, hydrogen-based systems, including electrolyzers, hydrogen tanks, and fuel cells, have gained increasing attention due to their ability to provide long-term energy storage and flexible energy conversion [5–8]. These systems enable surplus renewable energy to be stored and later converted into electricity, thereby improving system resilience and reducing energy curtailment.

Recent studies have demonstrated that integrating hydrogen technologies with renewable energy systems can significantly enhance system efficiency, operational flexibility, and sustainability [5, 9, 10]. In particular, hybrid configurations such as PV–WT–FC, PV–FC, and WT–FC systems have shown promising performance in terms of reliability, renewable penetration, and cost reduction [8,11–13]. Moreover, techno-economic analyses highlight the importance of hybrid systems in optimizing energy management and reducing operational costs while ensuring sustainable energy supply [5,9,10,14,15].

Despite significant progress in hybrid renewable energy systems (HRES), their optimal design and operation remain highly complex due to the need to simultaneously consider multiple and often conflicting objectives, including economic performance, system reliability, environmental impact, and grid stability under dynamic operating conditions [13, 16, 17]. This complexity is further amplified by the strong interdependence between system components. For example, the sizing of photovoltaic generation and hydrogen storage systems is inherently coupled, as increasing renewable capacity may reduce storage requirements, and vice versa [18]. As a result, multiple technically feasible configurations may exist, and optimization based on isolated criteria may not lead to a unique or practically optimal solution.

In addition, the performance of HRES is highly dependent on local meteorological conditions, such as solar irradiance, temperature, and wind speed, which directly affect renewable energy generation and system operation. Consequently, the optimal configuration of hybrid systems is strongly site-specific, requiring detailed modeling and long-term simulation under realistic operating conditions [19].

Although numerous studies have addressed the optimization of HRES, several important limitations remain. Most existing works focus primarily on individual study aspects, such as minimizing the levelized cost of energy (LCOE) or maximizing renewable energy penetration, without adequately considering operational constraints related to grid stability and system feasibility [14,17]. Furthermore, hydrogen storage systems are often modeled in a simplified manner, without fully capturing their dynamic interaction with renewable generation and grid exchange [10,15].

For instance, one study evaluated a hybrid system without energy storage in an urban context, focusing on economic and environmental performance. Although promising results were obtained in terms of cost and emissions, the absence of storage limited the system's ability to ensure reliability and stable operation [20].

In particular, hybrid configurations combining photovoltaic (PV), wind turbines (WT), and fuel cells (FC) have shown promising performance in terms of cost reduction and environmental impact [19, 21]. Recent studies have further confirmed that integrating hydrogen storage into such systems can significantly enhance performance by improving reliability and mitigating the intermittency of renewable energy sources [22]. However, reliability assessment is often limited to conventional indicators such as the Loss of Power Supply Probability (LPSP), which does not guarantee stable operation in grid-connected environments. The lack of explicit consideration of grid stability constraints, therefore, represents a critical gap in the current literature.

Another important limitation is the insufficient consideration of long-term system behavior. Many studies rely on simplified assumptions or short-term simulations, which do not fully capture the variability of renewable resources and system operation over time. This reduces the applicability of their findings for practical system design and deployment. In this context, there is a clear need for a comprehensive optimization framework capable of capturing the complex interactions between renewable generation, hydrogen storage, and grid dynamics, while ensuring both economic efficiency and operational feasibility.

To address these challenges, this study proposes an integrated techno-economic optimization framework for grid-connected hybrid renewable energy systems combining photovoltaic, wind, and hydrogen-based storage technologies. The proposed approach simultaneously considers economic performance, system reliability, and grid stability through a penalty-based multi-constraint formulation. Unlike conventional methods, this framework explicitly incorporates grid fluctuation constraints and models the coupled interaction between hydrogen storage and grid exchange, ensuring that the optimized system is both cost-effective and operationally viable.

The methodology is applied to a real case study in Dakhla, Morocco, using hourly meteorological data over a full year (8,760 h), enabling a realistic evaluation of system performance under actual operating conditions. Three system configurations (PV–WT–FC, PV–FC, and WT–FC) are comparatively analyzed to identify the most suitable design.

The main contributions of this work can be summarized as follows:

(i) Development of an integrated optimization framework combining economic, reliability, and grid stability criteria;
(ii) Introduction of a penalty-based objective function incorporating LPSP and grid fluctuation constraints;
(iii) Detailed modeling of hydrogen storage and its interaction with system components;
(iv) Implementation of a full-year simulation using site-specific data; and
(v) Comparative assessment of multiple hybrid system configurations under identical conditions.

Furthermore, although several studies have investigated hybrid renewable energy systems in different geographical contexts, limited research has focused on the Moroccan case, particularly for grid-connected PV–wind–hydrogen systems

integrating reliability and grid stability constraints. Most existing studies in Morocco are restricted to simplified configurations or focus primarily on economic or resource assessment aspects, without considering the combined effects of hydrogen storage, grid interaction, and operational constraints. Therefore, there remains a clear need for comprehensive, system-level optimization studies based on realistic Moroccan conditions, which can support the design of reliable and sustainable energy systems in the region.

2. Materials and methods

In this study, a comprehensive methodological framework was developed to design and evaluate a grid-connected hybrid renewable energy system integrating photovoltaic, wind, and hydrogen-based storage technologies. First, appropriate mathematical models for each system component, including PV panels, wind turbines, electrolyzer, hydrogen storage tank, and fuel cell, were selected from well-established literature and adapted using relevant technical parameters. All component models were then implemented within a unified MATLAB simulation environment, enabling dynamic interaction between renewable generation, storage, and grid exchange.

An energy management strategy was developed to govern system operation under different scenarios (surplus, deficit, and balanced conditions), ensuring efficient utilization of renewable energy and optimal use of hydrogen storage. The system design problem was formulated as a constrained optimization problem, where the objective function minimizes the total annual cost while incorporating reliability, grid stability, and environmental considerations. Key performance indicators—including economic metrics, loss of power supply probability (LPSP), grid fluctuation index, and renewable energy fraction—were evaluated over a full-year simulation (8,760 h) using site-specific meteorological and load data for Dakhla, Morocco.

Finally, the proposed framework was applied to analyze and compare the performance of several hybrid system configurations (PV–WT–FC, PV–FC, and WT–FC), allowing a detailed assessment of system behavior under realistic operating conditions. This integrated approach provides a robust basis for evaluating the effectiveness, feasibility, and sustainability of hybrid renewable energy systems in real-world applications.

2.1. Hybrid renewable energy system components modeling

This study proposes a grid-connected hybrid renewable energy system (HRES) integrating photovoltaic (PV) panels, wind turbines (WT), and a hydrogen-based storage subsystem composed of an electrolyzer, hydrogen storage tank, and fuel cell (FC), as illustrated in **Figure 1**.

The system is designed to ensure a reliable and efficient energy supply by coordinating renewable generation, hydrogen storage, and grid interaction. The modeling framework adopts a system-level integrated approach, where all components are dynamically coupled through energy balance equations and operational constraints.

Unlike conventional studies that treat system components independently, the present work explicitly considers: The interaction between renewable generation

and storage, the coupling between hydrogen production and consumption, and the bidirectional exchange with the utility grid.

This integrated formulation enables a more realistic representation of system behavior under varying operating conditions.

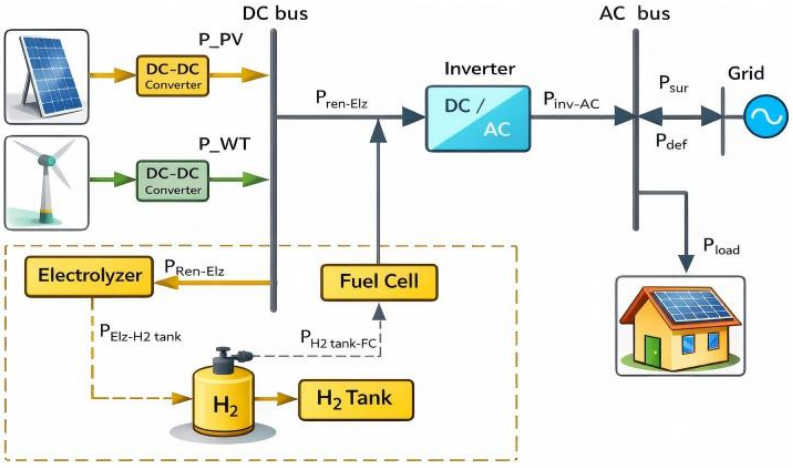

Figure 1. Schematic of the grid-connected PV/WT/FC hybrid energy system.

2.2. Photovoltaic (PV) model

The instantaneous power output of the photovoltaic (PV) system at time t is determined using Equation (1) [23].

$$P_{PV}(t) = P_r \times \eta_{pv} \times \frac{G(t)}{G_{ref}} \times [1 + \beta\,(T - T_{ref})] \quad (1)$$

In this model, $P_{PV}(t)$ indicates the real-time power output of the PV system (kW). The term η_{pv} defines the panel efficiency, and G(t) represents the incident solar radiation. The reference irradiance G_{ref} is specified under standard test conditions. The factor β is introduced to model the impact of temperature on PV performance, reflecting how power output responds to thermal deviations. In this context, T_{ref} defines the reference temperature, while T(t) indicates the cell's operating temperature and is obtained from Equation (2) [11]. Normal Operating Cell Temperature (NOCT) denotes the normal operating temperature of the PV cell.

$$T(t) = T_{amb}(t) + \frac{NOCT - 20}{1{,}000} \times G(t) \quad (2)$$

The overall PV power at time t is obtained by multiplying the number of PV units,denoted N_{PV}, by the output of a single unit, as follows [24]:

$$E_{PV}(t) = N_{PV} P_{PV}(t) \quad (3)$$

2.3. Wind turbine model

The mathematical representation of the wind turbine power output $P_{WT}(t)$ is given as follows [25]:

$$P_{WT}(t) = \begin{cases} 0, \text{ if } W_h(t) < W_{ci} \text{ or } W_h(t) > W_c \\ P_{rated} \frac{(W_h(t) - W_{ci})}{(W_r - W_{ci})} \text{ if } W_{ci} \leq W_h(t) < W_r \\ P_{rated}, \text{ if } W_h(t) \geq W_r \end{cases} \quad (4)$$

where P_{rated} denotes the rated turbine power, while W_{ci}, W_r, and W_{co} represent the cut-in, rated, and cut-off wind speeds, respectively.

Wind speed data measured at a reference height are converted to the wind turbine hub height using the power-law wind profile to account for vertical wind shear effects. This conversion ensures that the wind resource is accurately represented at the turbine operating level. In order to convert wind speed between heights, the power-law profile is adopted in this study, as shown in González Cusa et al.'s study [26]:

$$W_h(t) = W_{ref}(t) \left(\frac{H_h}{H_{ref}} \right)^n \quad (5)$$

$W_h(t)$ and $W_{ref}(t)$ denote hub and reference wind speeds, respectively. The parameter *n* is the wind shear exponent, which reflects the influence of terrain roughness and atmospheric stability on the vertical wind profile. For open and low-roughness terrains with good wind exposure, a commonly adopted value of $n = 0.14$ is used in this study [24].

In a similar manner, the total wind energy production is is evaluated as a function of the number of wind turbine units N_{WT}.

$$E_{WT}(t) = N_{WT} P_{WT}(t) \quad (6)$$

2.4. Electrolyzer model

The proposed HRES utilizes surplus renewable energy for hydrogen production via electrolysis. This is achieved by supplying a direct current to electrodes immersed in water, resulting in the generation of hydrogen and oxygen as described in reaction (R1) [27]. The corresponding electrical power transferred from the renewable sources to the hydrogen storage system via the electrolyzer, denoted $P_{Elz-tank}$ (kW), is given in Equation (7) [28].

$$P_{ren-Elz} + H_2O \longrightarrow H_2 + \frac{1}{2}O_2 \quad (R1)$$

$$P_{Elz-H_2tank} = P_{ren-Elz} \eta_{Elz} \quad (7)$$

where η_{Elz} defines the efficiency associated with the electrolyzer, which is assumed to remain constant throughout the simulation period, and $P_{ren-Elz}$ corresponds to the surplus renewable power supplied to it.

The amount of energy allocated to hydrogen production is determined by subtracting the load demand from the total renewable energy generation [3]. Furthermore, hydrogen production is constrained by the electrolyzer's rated capacity and the available storage in the hydrogen tank. The hydrogen produced at time t, $P_{H_2\_Produced}$, is limited by the available storage capacity as well as the power supplied to the electrolyzer. Accordingly, it can be expressed as [18]:

$$P_{H_2Produced}(t) = \min \left\{ E^{max}_{H_2\ tank} - E_{H_2\ tank}\ (t-1), \min\left(P_{ren\ -\ Elz}(t), P^{max}_{Elz}\right) \times \eta_{Elz} \right\} \quad (8)$$

where, $E_{H_{2tank}}^{max}$ represents the maximum storage capacity of the hydrogen tank, and $E_{H_2tank}(t-1)$ indicates the previously stored energy. $P_{ren-Elz}(t)$ denotes the surplus renewable power supplied to the electrolyzer, while P_{Elz}^{max} is its rated capacity.

2.5. Hydrogen storage tank modeling

The level of hydrogen energy in the tank changes continuously in response to production and usage processes. At time t, it is expressed as [12]:

$$E_{H_2\ tank}(t) = E_{H_2\ tank}\ (t-1) + \left(P_{Elz\ -\ H_2\ tank}(t) - \frac{P_{H_2\ tank\ -\ FC}\ (t)}{\eta_{HST}}\right)\Delta t \tag{9}$$

where the term $P_{Elz-H_2tank}(t)$ refers to the power supplied from the hydrogen tank to the fuel cell. Δt defines the time interval, and η_{HST} defines the storage efficiency, assumed constant throughout the analysis [27].

The energy stored in the hydrogen tank is continuously updated according to the balance between the hydrogen produced by the electrolyzer and the amount consumed by the fuel cell. An increase in stored energy occurs when excess renewable power is converted into hydrogen, whereas it decreases when hydrogen is utilized for power generation.

To quantify the stored hydrogen in physical terms, the energy content of the tank is converted into mass using the higher heating value of hydrogen. Accordingly, the hydrogen mass at time t is determined as [29]:

$$m_{H_2}(t) = \frac{E_{H_2\ tank}(t)}{HHVH_2} \tag{10}$$

where $HHVH_2$ represents the higher heating value of hydrogen, corresponding to the energy content per unit mass and is taken as 39.7 kWh/kg based on the adopted references [15, 27]. The stored hydrogen mass is restricted between predefined minimum and maximum limits, $m_{H_2\_min}$ and $m_{H_2\_max}$, to guarantee safe operation of the storage system. The following limits apply to stored hydrogen mass:

$$m_{H_2\_min}\ \leq m_{H_2}\ (t) \leq m_{H_2\_max} \tag{11}$$

2.6. Fuel cell stack modeling

In the fuel cell, hydrogen is converted into electrical energy through an electrochemical process. The overall reaction can be written as [11]:

$$2H_2 + O_2 \longrightarrow 2H_2O + P_{FC\ -\ inv} \tag{R2}$$

where P_{FC-inv} is the electrical power output of the fuel cell is given by [15]:

$$P_{FC\ -\ inv}\ = P_{H_2\ tank\ -\ FC}\ (t) \cdot \eta_{FC} \tag{12}$$

where η_{FC} represents the fuel cell efficiency, and $P_{H_2tank-FC}(t)$ denotes the power supplied from the hydrogen tank to the fuel cell.

The electrical power delivered by the fuel cell can also be expressed as a function of the hydrogen consumption $m_{H_{2,c}}$, which represents the amount required to meet the

load demand. It is given by [11]:

$$P_{FC-inv} = \frac{m_{H_{2,c}} \cdot HHVH_2}{\eta_{FC} \cdot \mu_{inv}} \tag{13}$$

2.7. Inverter modeling

In the proposed HRES, a Direct Current (DC)/Alternating Current (AC) inverter is employed to convert the direct current generated by the renewable sources and the fuel cell into alternating current suitable for load consumption. The inverter efficiency, μ_{inv}, is used to account for conversion losses and is assumed constant in this study [15].

Accordingly, the power supplied to the load can be expressed as [12]:

$$P_{inv-load} = (P_{FC-inv} + P_{ren-inv}) \times \mu_{inv} \tag{14}$$

The rated power of the inverter is determined based on the maximum load demand. $P_{inv,r}$ can be calculated using Equation (15) [30]:

$$P_{inv,r} = \frac{P_{load}^{Max}}{\mu_{inv}} \tag{15}$$

2.8. Optimization problem formulation

2.8.1. Decision variables

The design process of the proposed HRES is modeled as an optimization problem, where the capacities of the key components serve as decision variables. The objective is to determine the optimal configuration of these components that minimizes the total annualized cost while ensuring reliable and efficient system operation. To achieve this, the optimization process adjusts the capacities of the renewable generation units and the hydrogen storage subsystem. The corresponding decision vector is defined as:

$$X = [N_{WT}, N_{PV}, N_{Elz}, N_{Tank}, N_{FC}] \tag{16}$$

where $N_{WT}, N_{PV}, N_{Elz}, N_{Tank}$ and N_{FC} represent the variables for capacity of WT, PV panels, electrolyzer, hydrogen storage tank and FC.

2.8.2. Objective funciton

The optimization process aims to achieve minimum overall system cost while maintaining reliable and sustainable performance.This is achieved by minimizing the total annual cost (TAC), while accounting for penalties associated with reliability constraints. The objective function is therefore expressed as follows:

$$ob = \min \left[TAC(X) + C_{pc}(X) \right] \tag{17}$$

where TAC is the total annual cost and C_{pc} represent the penalty cost associated with constraint violations.

The total annual cost, TAC, is calculated by summing the annualized cost of the hybrid system, including capital, operation and maintenance, replacement costs, and salvage value of all HRES component including WT, PV panels, electrolyzer, hydrogen

storage tank and FC [28]. In addition, since the system operates in a grid-connected mode, the cost function incorporates the economic impact of energy exchanges with the utility grid.

Depending on the balance between generation and demand, the system may either import energy from the grid or export excess power. These exchanges are evaluated based on predefined electricity tariffs, where the cost of imported energy is determined by the amount of energy purchased from the grid, while exported energy generates revenue. Accordingly, both C_{grid_s} and C_{grid_p} are included in the overall cost formulation to ensure an accurate representation of the system's economic performance. As a result, the overall cost formulation can be expressed as follows [3]:

$$TAC(X) = \sum_{k=1}^{N_{Component}} N_K TC_K + C_{grid_s} - C_{grid_p} \tag{18}$$

where, N_K and TC_K denote denote the number and annualized cost of component K, respectively. The annualized cost of each component is calculated as follows [31]:

$$TC_K = (Capital_K + O\&M_K + Replacement_K - Salvage_K) \tag{19}$$

The capital investment of each subsystem i is converted into an equivalent annual cost by applying the capital recovery factor, which accounts for both the interest rate and component lifetime [15]:

$$Capital_K = C_{cap,K} \times CRF(r, L_{HRES}) \tag{20}$$

where, r denotes the effective discount rate, which accounts for the influence of inflation, and L_{HRES} represents the operational lifetime of the hybrid system. While the CRF (d,Y_i) is the capital recovery factor of the HRES and is calculated using Equation (21) [11,15].

$$CRF\,(d, Y_i) = \frac{d.(1+d)^{Y_i}}{(1+d)^{Y_i}-1} \tag{21}$$

In this context, d refers to the rate of interest, which includes the impact of inflation, while Y_i represents the complete lifespan of the hybrid system.

The annualized replacement cost of subsystem i is quantified according to the following formulation [15]:

$$Replacement_K = C_{rep,K} \times \frac{(L_{HRES} - L_i)}{L_i} \tag{22}$$

The overall project lifetime of the hybrid renewable system, represented by L_{HRES}, is set to 25 years. Therefore, replacement costs are considered for all components whose lifetimes are less than this period.

The hybrid system exchanges energy with the utility grid depending on the generation–demand balance, exporting surplus power and importing deficit power. These exchanges are economically evaluated as:

$$C_{grid\_imp} = E_{grid\_imp} \times \lambda_{imp} \tag{23}$$

$$C_{grid\_exp} = E_{grid\_exp} \times \lambda_{exp} \tag{24}$$

The economic interaction between the hybrid system and the utility grid is modeled using fixed electricity tariffs. The unit cost of electricity imported from the grid is denoted by λ_{imp}, while the selling tariff for electricity exported to the grid is represented by λ_{exp}. The total electrical energy exchanged with the grid is quantified by E_{grid_imp} for imported energy and E_{grid_exp} for exported energy.

2.8.3. Economic metrics

These economic indicators play a fundamental role in evaluating the financial performance of the proposed hybrid energy system, as they directly support the cost–benefit assessment and the determination of overall economic feasibility. Three key parameters are considered: the total annual cost (TAC), penalty costs, and the Levelized Cost of Energy (LCOE).

Equation (24) is used to calculate LCOE based on TAC, as detailed in the study of Drici et al. [18]:

$$\mathrm{LCOE} = \frac{\mathrm{TAC}}{\sum_{t=1}^{t=8,760} E_{total}} \tag{25}$$

where E_{total} represents the total energy produced by the HRES.

2.8.4. Reliability metrics

In the proposed framework, the penalty cost C_{pc} quantifies the system's deviation from the desired reliability level, measured by the Loss of Power Supply Probability (LPSP), and from acceptable grid interaction behavior, represented by the power fluctuation index F_{grid}. According to the recommendations reported in the studies of Sultan et al. and Mohamed et al. [15,32] the LPSP must not exceed a predefined upper bound $\beta_L = 0.01$. In addition, the surplus power fluctuation rate F_{grid} is constrained by a threshold B_g, which is limited to 33% of the installed system capacity within a 10-min time interval. Due to the hourly resolution of the available data, the grid fluctuation index is approximated using hourly variations, assuming constant behavior within each hour. This simplification is commonly adopted but may slightly underestimate short-term fluctuations.

The penalty cost is expressed as follows [32]:

$$C_{pc} = C_{pc1}\left(\mathrm{LPSP} - \beta_L\right)\sum_{i=1}^{N} P_{load}\left(t_i\right) + C_{pc2}\frac{F_{grid} - B_g}{B_g} \times 100 \tag{26}$$

where $P_{load}\left(t_i\right)$ is the penalty coefficient associated with reliability violation (C_{pc1}= 100 \$/kWh) and C_{pc2} is the penalty coefficient related to grid power fluctuation violation (C_{pc2} = 50,000/%)

$$\mathrm{LPSP} = \frac{\sum_{t=1}^{t=8,760}\left(P_{load}(t) - P_{WT}(t) - P_{PV}(t) - P_{FC\ -\ inv}\right)}{\sum_{t=1}^{t=8,760} P_{load}(t)} \tag{27}$$

The rate of power fluctuation F_{grid}(unitless) can be expressed as follows [31]:

$$F_{grid} = \frac{P_{sur,max} - P_{sur,min}}{\Delta t} \tag{28}$$

where $P_{sur,max}$ are the maximum and minimum surplus powers exchanged with the grid during the time interval Δt.

To ensure that renewable energy sources supply the majority of the load demand,

a relative load fluctuation index, denoted as D_{load}, is introduced.

This index evaluates the degree of mismatch between renewable power generation and load consumption, thereby reflecting the effectiveness of renewable energy utilization within the system. Following the methodology reported in the study of Mohamed et al. [32], D_{load} is defined as:

$$D_{load} = \frac{\sqrt{\frac{1}{N}\sum_{t=1}^{N}[P_{PV}(t)+P_{WT}(t)-P_{load}(t)]^2}}{\overline{P_{load}}} \tag{29}$$

where $\overline{P_{load}}$ represents the average load demand over the considered period, and N is the total number of time steps (8,760). According to the analysis reported in the studies of Sultan et al., Mohamed et al. and Xu et al. [15, 32, 33], the relative load fluctuation index D_{load} serves as a key indicator of renewable energy utilization efficiency. A lower value of this index indicates a stronger alignment between renewable power generation and load demand, which reflects a higher penetration of photovoltaic and wind resources in the overall energy mix. When the index remains below the predefined reference threshold $\varepsilon_L = 2$, the system can be regarded as operating predominantly on renewable energy, with only minimal reliance on auxiliary or external power sources. Maintaining D_{load} within the allowable range confirms that renewable generation closely matches load demand, thereby enhancing energy utilization, reducing curtailment, and demonstrating the effectiveness of the proposed hybrid system configuration.

2.8.5. Environmental indicator

The reduction in carbon dioxide emissions achieved by the proposed hybrid system can be evaluated as [11]:

$$t_{CO_2} = EF \cdot E_{total} \tag{30}$$

where t_{CO_2} denotes the amount of CO_2 emissions avoided, EF is the emission factor expressed in tons of CO_2 per unit of generated energy, and E_{total} represents the annual energy production of the HRES. In addition, the Renewable Energy Fraction (REF) is used to quantify the share of the load supplied by renewable sources. It is defined as [3]:

$$REF = 1 - \frac{\sum_{t=1}^{8,760} P_{defit}}{\sum_{t=1}^{8,760} P_{ren}} \tag{31}$$

where P_{defit} and P_{ren} represent the total power deficit and the total renewable power generation, respectively. In the proposed grid-connected HRES, any deficit in power is compensated by importing electricity from the utility grid. Therefore, the imported grid energy can be used as an equivalent measure of the deficit when evaluating this factor.

2.8.6. Constraints

A number of technical and operational limitations are imposed on the optimization problem to guarantee feasible and reliable operation of the HRES. These constraints define the allowable ranges of the decision variables as well as the system performance requirements.

The bounds of the decision variables are defined as follows:

$$0 \leq N_{WT} \leq N_{WT\_max}$$
$$0 \leq N_{PV} \leq N_{PV\_max}$$
$$0 \leq N_{Elz} \leq N_{Elz\_max}$$
$$0 \leq N_{tank} \leq N_{tank\_max}$$
$$0 \leq N_{FC} \leq N_{FC\_max}$$

In addition, the hybrid system must satisfy other performance constraints [3]:

$$LPSP \leq 0.01$$
$$REF \geq 0.60$$
$$D_{gs} \leq 0.33$$
$$D_{load} \leq 2$$

2.9. Operational simulation and energy management strategy

The operational strategy of the proposed hybrid PV–WT–FC system is based on continuous monitoring of the renewable generation and load demand to ensure optimal power management. At each time step, the total renewable power$P_{ren}(t)$ and the load demand $P_{load}(t)$ are measured and compared, considering inverter efficiency. When the renewable generation equals the load requirement, the load is fully supplied by the photovoltaic and wind sources, and the fuel cell remains inactive. If the renewable generation exceeds the load demand, the surplus power is directed to the electrolyzer for hydrogen production, while any excess beyond the electrolyzer capacity is exported to the utility grid. Conversely, when the renewable generation is insufficient to meet the load, the deficit power is supplied by the fuel cell using the hydrogen stored in the tank. The hydrogen tank level is continuously checked to ensure operation within its allowable limits. If the fuel cell cannot fully compensate for the deficit due to capacity or storage constraints, the remaining power shortage is covered by the grid. This hierarchical control strategy prioritizes renewable energy utilization, promotes efficient hydrogen storage and recovery, and minimizes grid dependency while guaranteeing an uninterrupted power supply.

The system operates according to the following scenarios:

Case 1: Renewable generation equals load

If $P_{ren}(t) = \frac{P_{load}(t)}{\mu_{inv}}$,

the load is fully supplied by renewable sources, and the fuel cell remains inactive.

Case 2: Renewable surplus

If $P_{ren}(t) > \frac{P_{load}(t)}{\mu_{inv}}$,

the surplus power is sent to the electrolyzer to produce hydrogen. Any excess power beyond the electrolyzer capacity is exported to the grid.

$$P_{surp}(t) = P_{ren}(t) \times \mu_{inv} - P_{load}(t) \tag{32}$$

Case 3: Renewable deficit

If $P_{ren}(t) < \frac{P_{load}(t)}{\mu_{inv}}$,

the power deficit is supplied by the fuel cell. If the fuel cell capacity is insufficient, the remaining shortage is covered by the utility grid.

$$P_{defit}(t) = P_{load}(t) - (P_{ren-inv} + P_{FC-inv}) \times \mu_{inv} \quad (33)$$

Figure 2 presents the overall optimization framework and operational strategy of the proposed grid-connected hybrid renewable energy system (HRES). The procedure begins with the initialization of input parameters, including hourly meteorological data (solar irradiance, wind speed, and ambient temperature), electrical load demand, and the technical and economic specifications of system components. Subsequently, the appropriate system configuration is selected from candidate structures (PV–WT–FC, PV–FC, and WT–FC). For each configuration, component capacities are optimized to achieve the best techno-economic performance. Finally, the selected system is evaluated using an optimization algorithm, followed by a simulation stage (node A) to assess system performance and determine the optimal design solution.

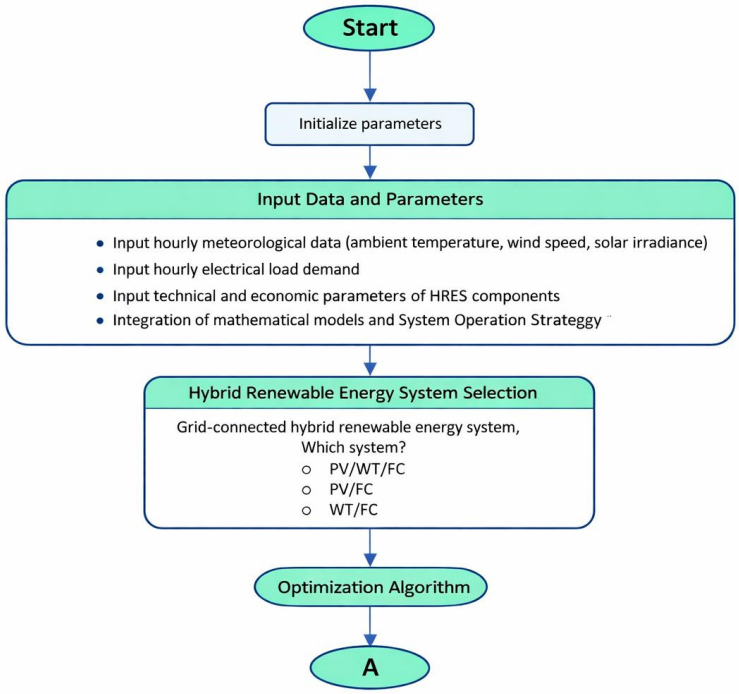

Figure 2. Overall optimization framework.

The second part of the flowchart depicted in **Figure 3**, which represents the hourly operational simulation and energy management strategy of the proposed HRES. The system is simulated over an annual horizon of 8,760 hourly time steps. At each time step, the power generated by the photovoltaic array and wind turbines is computed to estimate the total available renewable energy. The operational strategy described previously is activated, and the system energy balance is determined.

After completing the yearly simulation, several performance indicators are calculated to evaluate the reliability and operational behavior of the system. These indicators include the Loss of Power Supply Probability (LPSP), the load fluctuation index D_{load}, and the grid fluctuation index D_{gs}.

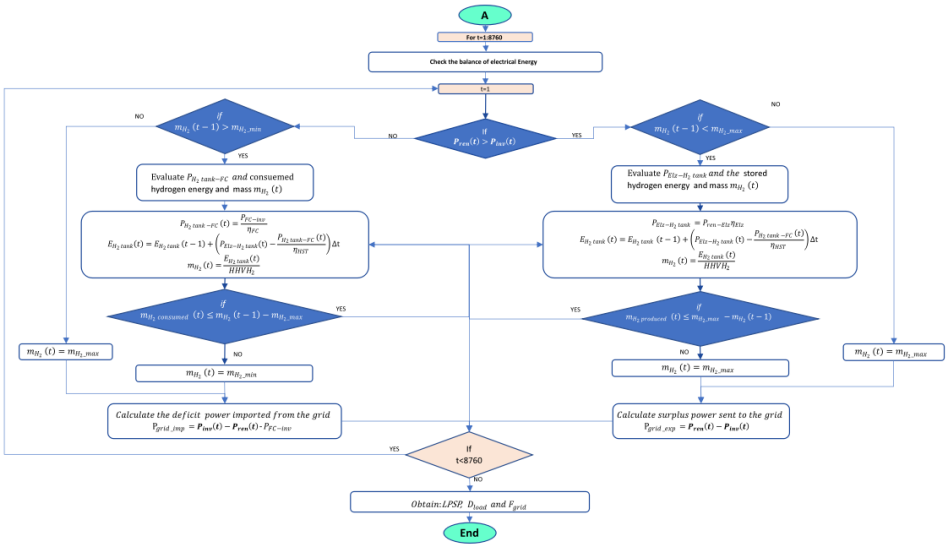

Figure 3. Flowchart of operating management strategy.

To ensure that the obtained solution satisfies all operational requirements, a penalty-based constraint handling mechanism is incorporated into the optimization framework. When reliability or operational constraints are violated, additional penalty costs are introduced into the objective function. Consequently, the optimization problem aims to minimize the total annualized system cost combined with the associated penalty costs.

The optimization algorithm iteratively updates the decision variables corresponding to the capacities of the system components and repeats the simulation procedure until convergence is achieved. The final result corresponds to the system configuration that provides the minimum objective function value while satisfying all technical and operational constraints, thereby ensuring reliable and economically efficient operation of the grid-connected hybrid renewable energy system.

2.10. Simulation analysis of HRES

2.10.1. Study area location

This study presents a techno-economic evaluation, optimization, and comparative analysis of several grid-connected hybrid renewable energy configurations, including PV–wind–Fuel Cell, PV–Fuel Cell, and Wind–Fuel Cell systems. These systems are designed to supply electricity to a load within a microgrid located in the southern region of Morocco, specifically in the province of Dakhla, as illustrated in **Figure 4**. The geographical coordinates of the study site are approximately 23.41° longitude and 15.58° latitude.

2.10.2. Load profile data

The annual electrical load profile of the microgrid located in Dakhla is presented in **Figure 5**. It illustrates the continuous variation of electricity demand over 8,760 h throughout the year. The profile exhibits temporal fluctuations, with alternating periods of low and high consumption, reflecting typical daily and seasonal variations. This load profile provides a representative basis for evaluating system performance under realistic operating conditions.

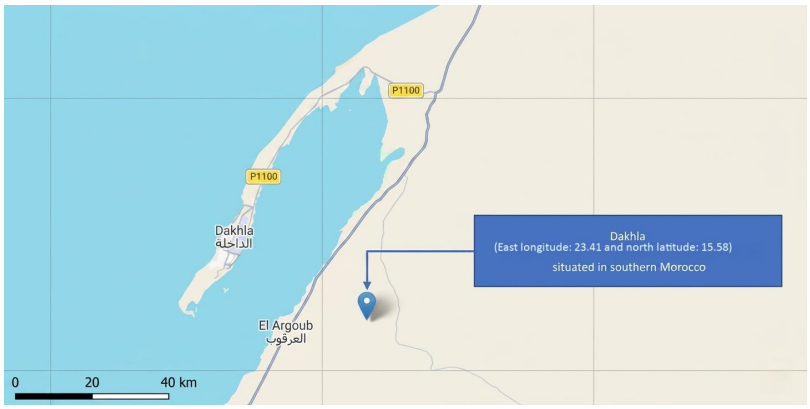

Figure 4. Location of the proposed grid-connected system.

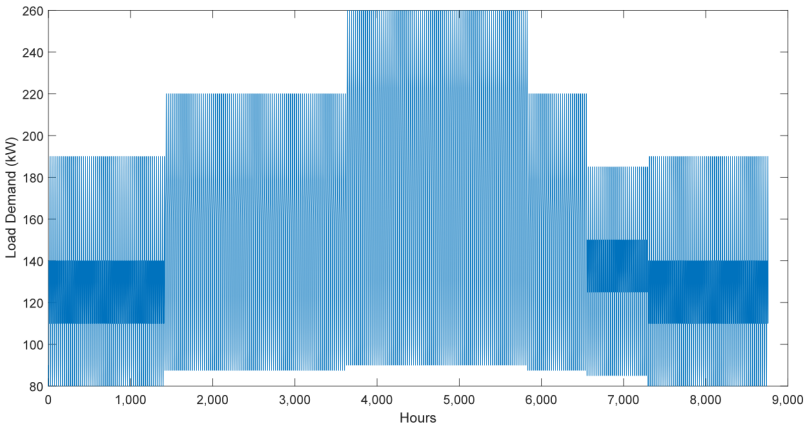

Figure 5. Annual hourly electrical load profile (8,760 h) for the studied system in Dakhla.

2.10.3. Meteorological data

In this study, the System Advisor Model (SAM) software is used exclusively to determine the solar irradiance incident on the photovoltaic modules. The available solar radiation data, typically provided for horizontal surfaces, are imported into SAM in Excel format together with site-specific parameters such as latitude, longitude, and PV module tilt angle. Using its built-in solar geometry and transposition models, SAM converts the horizontal irradiance into the effective irradiance received by the tilted photovoltaic panels. The resulting time-series profile of the incident solar irradiance, denoted G(t) (W/m^2), is then exported in CSV format and integrated into the hybrid system simulation framework. This approach provides a practical and computationally efficient method for solar resource assessment, while avoiding the need to implement complex solar radiation modeling procedures and ensuring the reliability of the overall system analysis. **Figure 6** illustrates the temporal variation of key meteorological parameters at the study site, including ambient temperature, wind speed, and solar irradiance over an annual period. The ambient temperature profile shows a clear diurnal and seasonal trend, with values ranging from approximately 10 °C to 40 °C. Higher temperatures are observed during the middle of the year, indicating strong seasonal influence, while short-term fluctuations reflect daily thermal cycles. The solar irradiance exhibits a highly regular and repetitive pattern, varying from nearly 0 to about 1,100 W/m^2. The presence of sharp, periodic peaks followed by near-zero values clearly reflects the day–night cycle. The consistency of these peaks, with frequent values

exceeding 800 W/m^2, highlights the strong solar potential of the site. In contrast, the wind speed displays a more stochastic behavior, generally fluctuating between 2 m/s and 9 m/s, with intermittent peaks.

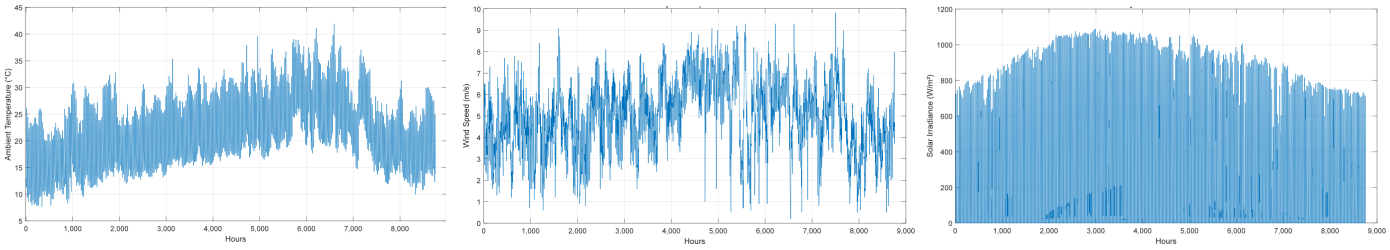

(a) **(b)** **(c)**

Figure 6. **(a)** Hourly ambient temperature profile of the study area; **(b)** Corresponding wind speed variation at the selected location; **(c)** The estimated solar irradiance on the PV array.

By combining accurate solar irradiance transformation and wind speed extrapolation, the proposed methodology ensures reliable meteorological data preprocessing, thereby improving the credibility of the performance evaluation and optimization of the hybrid PV/Wind/Fuel Cell energy system.

2.10.4. Optimization algorithm selection

Particle Swarm Optimization (PSO) is a population-based global optimization technique introduced by Kennedy and Eberhart in 1995. The method is inspired by the collective behavior observed in nature, such as bird flocking, where individuals interact and adapt based on both their own experience and that of the group [34]. In PSO, a set of candidate solutions, referred to as particles, forms a swarm that explores the search space collaboratively.

The optimization process is carried out iteratively through three main stages [3,35]. First, a population of particles is generated with random positions and velocities within the defined search space, and the objective function is evaluated for each particle. Then, the best positions are updated by comparing the current solution with both the particle's personal best and the global best among all particles. Finally, the velocity and position of each particle are adjusted using the PSO update equations, allowing the swarm to progressively move toward the optimal solution. The process continues for several iterations until the algorithm arrives at a stopping criterion.

Each particle i represents a candidate solution in the search space, defined by its position $x_i(k)$ and velocity $v_i(k)$ at iteration k. In addition, each particle stores two reference positions: the personal best position $P_{best,i}(k)$ corresponding to the best solution previously found by the particle, and the global best position $G_{best,i}(k)$ corresponding to the best solution identified by the entire swarm.

Initially, a population of N_P particles is randomly generated within the feasible search space. For each particle, the hybrid system is simulated using its initial position $x_i(0)$ and key performance indicators, including the TAC, LPSP, F_{grid}, D_{load} and C_{pc} are computed. The objective function is defined as described in Equation (16).

As the algorithm progresses, particles update their trajectories by considering three main influences: their previous motion, their own experience, and the collective experience of the swarm. At each iteration k, the velocity and position of particle i are

updated according to:

$$v_i(k+1) = \omega v_i(k) + c_1 r_1 \left(P_{best,\,i}(k) - x_i(k)\right) + c_2 r_2 \left(G_{best,\,i}(k) - x_i(k)\right) \quad (34)$$

$$x_i(k+1) = x_i(k) + v_i(k+1) \quad (35)$$

In these equations, $v_i(k)$ and $x_i(k)$ denote the velocity and position of particle i at iteration k, respectively. The parameter ω is the inertia weight that controls the influence of the previous velocity, promoting exploration of the search space. The coefficients c_1 and c_2 represent the cognitive and social components, guiding the particle toward its personal best and the global best positions. The random variables r_1 and r_2 are uniformly distributed in the interval [0,1], introducing stochastic behavior into the search process. Through successive iterations, particles adjust their positions and share information, enabling the swarm to gradually converge toward an optimal or near-optimal solution. The process continues until a predefined stopping criterion, such as the maximum number of iterations, is reached.

3. Results and discussion

3.1. Optimization results and system sizing

The optimization procedure was carried out over 100 iterations, where each run was performed independently. The best solution was selected based on the minimum value of the objective (fitness) function. The Particle Swarm Optimization (PSO) algorithm was implemented using a population size of 60 particles and a maximum of 100 iterations. This optimization framework was applied to three different system configurations: PV–WT–FC, WT–FC, and PV–FC, in order to evaluate their relative performance and identify the most suitable design.

In this section, the results corresponding to the best-performing runs of the PSO algorithm are presented. The convergence curves of the PSO algorithm for the different hybrid system configurations are presented in **Figure 7**. It can be observed that, for all cases, the algorithm exhibits a rapid decrease in the fitness value during the initial iterations, followed by a gradual stabilization, indicating effective exploration and exploitation capabilities. The PSO algorithm successfully converges toward optimal or near-optimal solutions within a limited number of iterations, demonstrating its robustness and efficiency in solving the hybrid system optimization problem. Among the studied configurations, the PV–WT–FC system achieves the lowest fitness value, highlighting its superior economic performance compared to the PV–FC and WT–FC configurations.

The optimal component sizes and associated economic metrics for each configuration are summarized in **Table 1**. The PSO algorithm successfully determines the most suitable combination of system components for each configuration. The optimal configurations obtained for the three hybrid systems can be expressed in terms of their component capacities. For instance, the optimal PV–WT–FC system consists of 530 kW of PV, 140 kW of wind capacity, a 199.1 kW electrolyzer, a 100-kW fuel cell, and a hydrogen storage capacity of 780 kWh (19.65 kg). while for the PV–FC

configuration, the system includes a photovoltaic capacity of 670 kW, an electrolyzer rated at 276.1 kW, a hydrogen storage capacity of 1,490.5 kWh (37.54 kg), and a fuel cell rated at 100 kW. **Figure 8** presents a Comparison of component capacities for PV–WT–FC and PV–FC configurations obtained from the optimization algorithm.

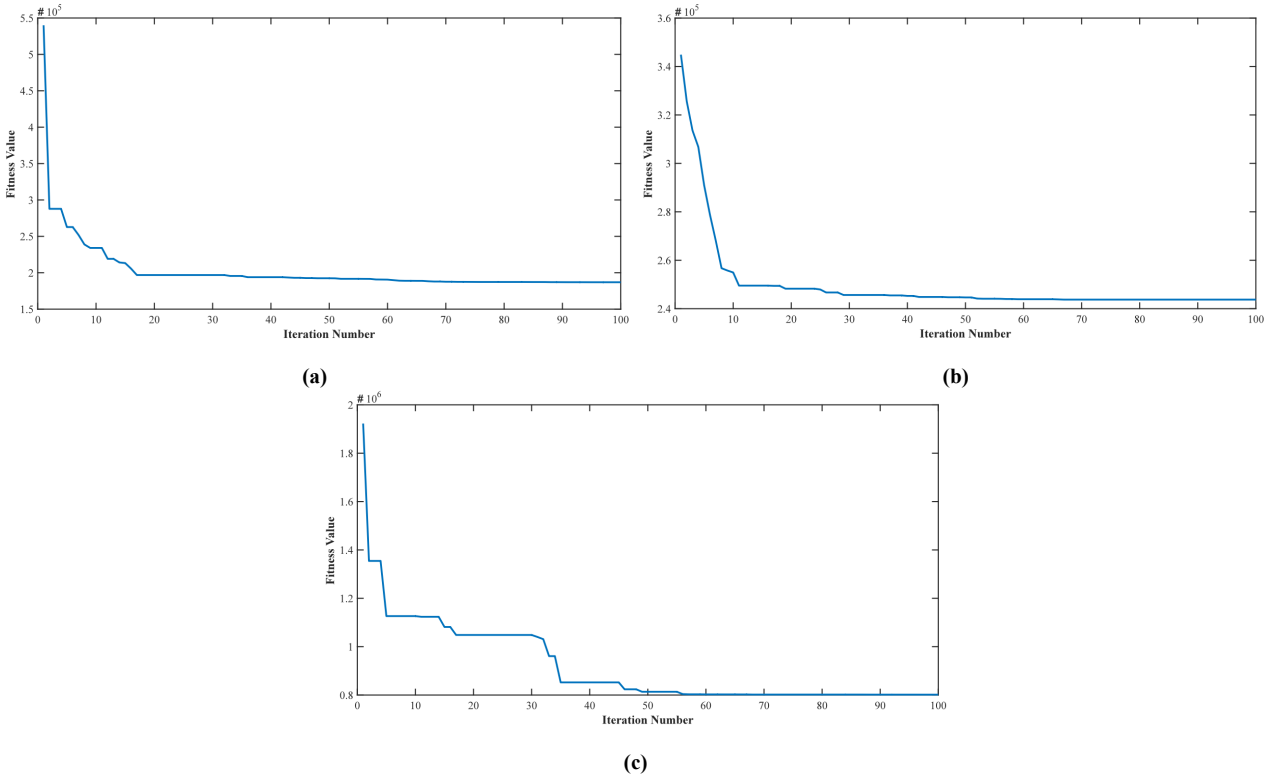

Figure 7. Convergence curve for: **(a)** Convergence curve of PV–WT–FV; **(b)** Convergence curve of PV–FC; **(c)** Convergence curve of WT–FC.

Table 1. Optimal system configuration.

Configuration	PV–WT–FC	WT–FC	PV–FC
Pramater			
LCOE ($/kWh)	0.1472	0.1164*	0.1964
Total annual cost ($)	186,957	151,412	255,425
Penalty cost ($)	0	700,588	0
Objective function value ($)	186,957	852,001	255,425
Component			
Wind turbines unit	70	171	0
Wind capacity (kW)	140	342	0
PV units	265	0	335
PV capacity (kW)	530	0	670
Electrolyzer (kW)	199.1	152.6	276.1
Fuel cell (kW)	100	149.1	100
H_2 storage (kWh)	780	21,020.1	1,490.5
H_2 storage (kg)	19.65	529.47	37.54

Note: ∗ The penalty costs are not included in the reported total annual cost, but are introduced separately to account for system stability and reliability.

From an economic perspective, significant differences are observed among the configurations. While the WT–FC system achieves the lowest Levelized Cost of Energy (LCOE) at $0.1164/kWh, it incurs a substantial penalty cost of $700,588 due to grid

instability. When this penalty is incorporated into the objective function, the total cost for the WT–FC system rises to $852,001, which is more than three times higher than that of the other configurations. This result highlights the critical importance of including reliability and grid interaction constraints in the optimization framework, as a purely LCOE-based analysis would be misleading. Conversely, the PV–FC system exhibits the highest LCOE ($0.1964/kWh), driven by the high investment cost of its 670 kW PV array and a greater reliance on grid purchases.

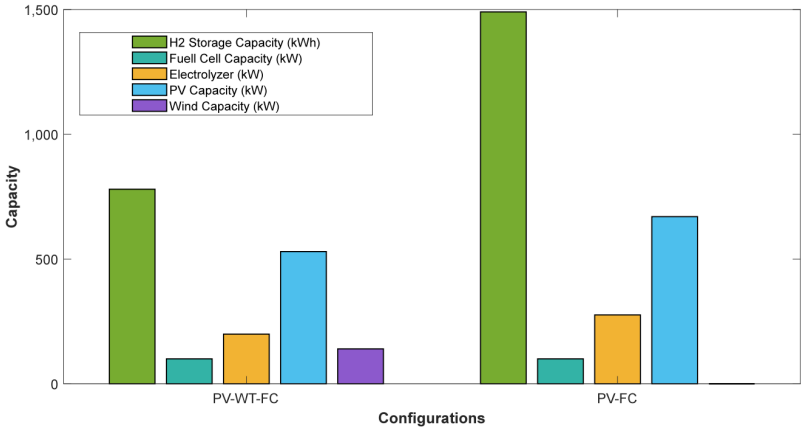

Figure 8. Component capacities for PV–WT–FC and PV–FC configurations.

3.2. System reliability and grid interaction

System reliability and grid compatibility were assessed using the Loss of Power Supply Probability (LPSP), renewable fraction (REF), grid fluctuation index (D_{gs}), and load fluctuation index (D_{load}), as detailed in **Table 2** and illustrated in **Figure 9**. All configurations demonstrate near-zero LPSP values, confirming their high reliability in meeting the load demand.

Table 2. Reliability indicators.

Metric	PV–WT–FC	WT–FC	PV–FC
Renewable fraction (%)	88.32	96.54	60.00
LPSP	0.0000	0.0000	0.0001
Grid fluctuation index (Dgs)	0.33	0.376	0.33
Load fluctuation index (Dload)	0.988	0.814	1.115

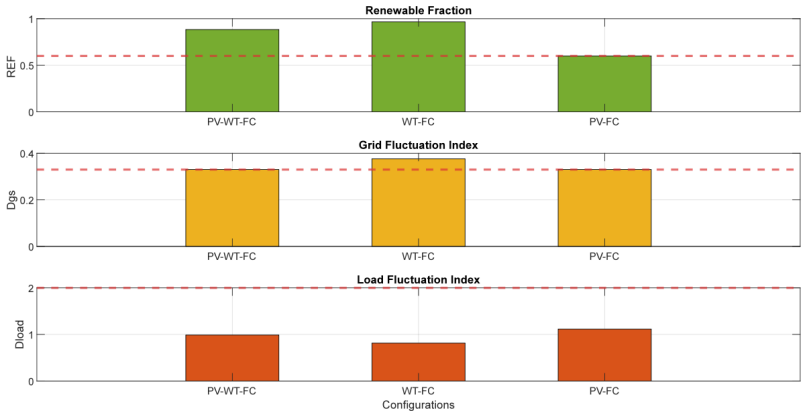

Figure 9. Reliability indicators comparison across configurations.

Figure 9 further illustrates the comparative performance of the studied configurations in terms of renewable fraction (REF), grid fluctuation index (D_{gs}), and load fluctuation index (D_{load}), relative to their respective operational constraints. All configurations satisfy the minimum REF requirement, with the WT–FC system achieving the highest renewable penetration. Nevertheless, this advantage is offset by its inability to maintain grid stability, as evidenced by its violation of the D_{gs} constraint.

In contrast, the PV–WT–FC and PV–FC configurations remain within the acceptable D_{gs} limits, demonstrating enhanced grid compatibility. This improvement can be attributed to the stabilizing effect of photovoltaic generation, which mitigates the variability associated with wind power. Additionally, all configurations comply with the D_{load} constraint, confirming their capability to ensure stable load supply.

Importantly, the discrepancy observed in the WT–FC configuration where D_{load} remains acceptable while D_{gs} exceeds its limit highlights the fundamental distinction between load reliability and grid stability. Overall, the PV–WT–FC configuration achieves the most balanced performance, ensuring high reliability, acceptable renewable contribution, and stable interaction with the grid.

3.3. Environmental impact

The environmental analysis presented in **Table 3** shows that all configurations significantly reduce CO_2 emissions. The WT–FC system achieves the highest savings (868 t/year), followed by the PV–WT–FC system (778 t/year). The PV–FC configuration provides lower emission reduction (534 t/year) due to its limited renewable contribution. Overall, hybrid systems with higher renewable integration offer greater environmental benefits.

Table 3. Environmental index.

Configuration	CO_2 emissions saved (t/year)
PV–WT–FC	778
WT–FC	868
PV–FC	534

3.4. Economic analysis and cost distribution

To better understand annual system costs by category, **Figure 10** provides a breakdown for each subsystem, revealing the overall cost allocation. Pie charts in the **Figure 10** show the percentage of total annualized cost for each subsystem across the three hybrid configurations: PV–WT–FC, WT–FC, and PV–FC. Additionally, bar charts illustrate the distribution of capital, O&M, and replacement costs for system components in all configurations.

The pie charts show that the main generation technology accounts for the largest cost share: PV represents 52% of costs in the PV–WT–FC system and 65% in the PV–FC system, while wind power accounts for 51% of the WT–FC system. Hydrogen contributes substantially across all configurations (26–46%), whereas inverter costs remain small (3–4%). Capital cost is the dominant contributor across all generator

technologies, especially for PV and wind power. Replacement costs are largely tied to hydrogen components (fuel cells and electrolyzers) due to their shorter lifespans, while O&M and other components play a minor role. The PV–WT–FC system shows the most balanced cost distribution, underscoring the benefit of integrating multiple renewable sources.

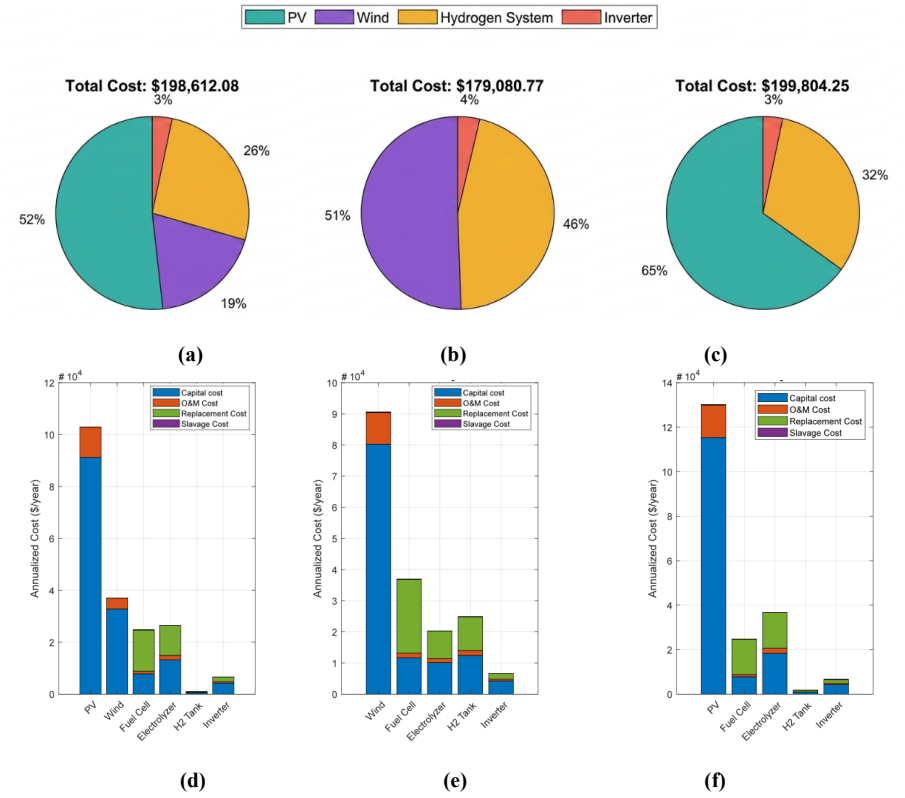

Figure 10. Cost distribution of: **(a)** PV–wind–FC; **(b)** Wind–FC; **(c)** PV–FC; distribution of capital, O&M, and replacement costs of: **(d)** PV–wind–FC; **(e)** Wind–FC; **(f)** PV–FC.

The economic benefit of grid interaction is quantified in **Table 4**. Enabling electricity export consistently improves economic performance across all configurations. For the PV–WT–FC system, the annual cost decreases from \$198,612 to \$186,957, and the LCOE from \$0.1527/kWh to \$0.1437/kWh. This confirms that the ability to sell surplus renewable energy significantly enhances the economic viability of these hybrid systems.

Table 4. Annual system cost and levelized cost of energy (LCOE) for Hybrid configurations with and without grid trading.

System	Scenario	Annual cost ($/yr)	LCOE ($/kWh)
PV–wind–FC	Grid trading allowed	186,957	0.1437
	No selling to grid	198,612	0.1527
Wind–FC	Grid trading allowed	151,412	0.1164
	No selling to grid	179,081	0.1377
PV–FC	Grid trading allowed	255,425	0.1964
	No selling to grid	264,887	0.2037

Figure 11 presents the distribution of the annualized cost (TAC) of the proposed grid-connected PV–WT–Fuel Cell hybrid system, highlighting the economic

contribution of each component. The results indicate that the PV subsystem accounts for the largest share of the total cost due to its high installed capacity required to ensure adequate energy production, followed by the wind subsystem, while the hydrogen subsystem introduces additional costs but provides essential flexibility and reliability through energy storage and conversion. In contrast, the inverter contributes only a minor portion of the total cost, whereas the grid interaction yields a negative cost due to revenue generated from excess energy export. From an economic perspective, these results demonstrate that although renewable generation and hydrogen technologies require significant initial investment, the integration of PV, wind, and fuel cell systems enables efficient energy utilization, reduces dependence on external supply, and enhances profitability through grid sales, thereby improving the overall cost-effectiveness of the proposed hybrid system.

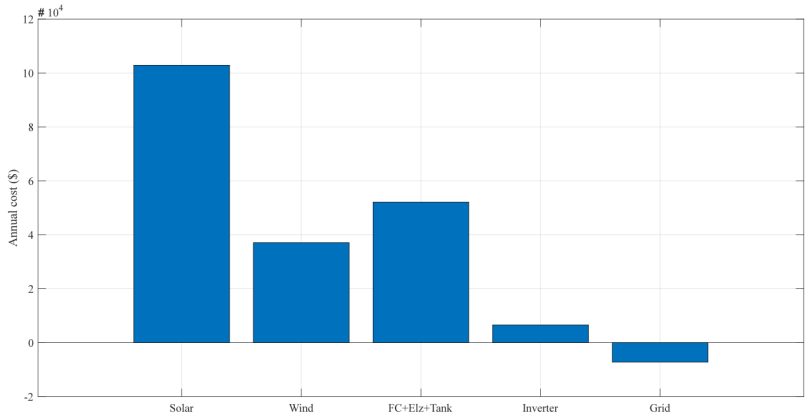

Figure 11. Annual cost breakdown of PV–WT–FC.

3.5. Energy management and operational dynamics

Figure 12 compares the energy production and grid interaction of the three hybrid systems (PV–wind–FC, Wind–FC, and PV–FC), showing renewable generation, fuel cell output, grid purchases, and grid exports. The results indicate that the WT–FC system produces the highest renewable energy, followed by the PV–WT–FC system, both of which export significant surplus electricity to the grid. In contrast, the PV–FC system generates less renewable energy and relies heavily on grid purchases, while the fuel cell plays a larger role in compensating for solar variability. Overall, **Figure 12** highlights that combining wind and solar resources improves energy balance and reduces dependence on grid electricity.

The energy management strategy of the optimal PV–WT–FC configuration was analyzed in detail. **Figure 13** illustrates the daily energy contributions of the PV, wind, fuel cell, and grid within the proposed hybrid system, highlighting their complementary roles in meeting the load demand. The PV generation shows a relatively stable trend, while wind power exhibits significant variability due to changing wind conditions. The fuel cell ensures continuity of supply by compensating for periods of low renewable generation through the use of stored hydrogen. Additionally, the grid provides supplementary support when necessary, ensuring a reliable and balanced energy supply throughout the year.

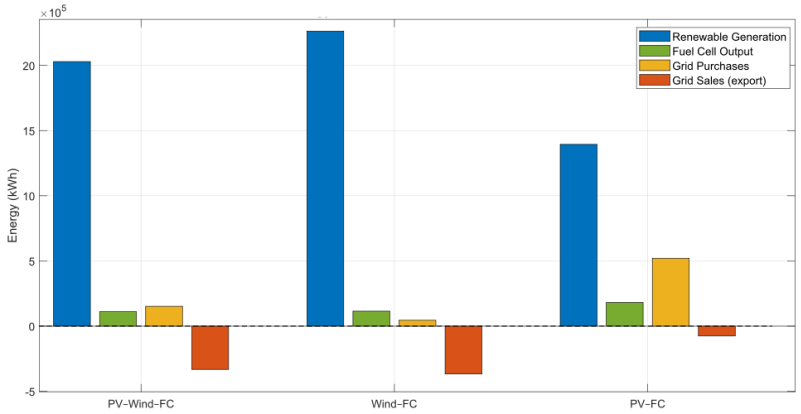

Figure 12. Energy production and grid interaction.

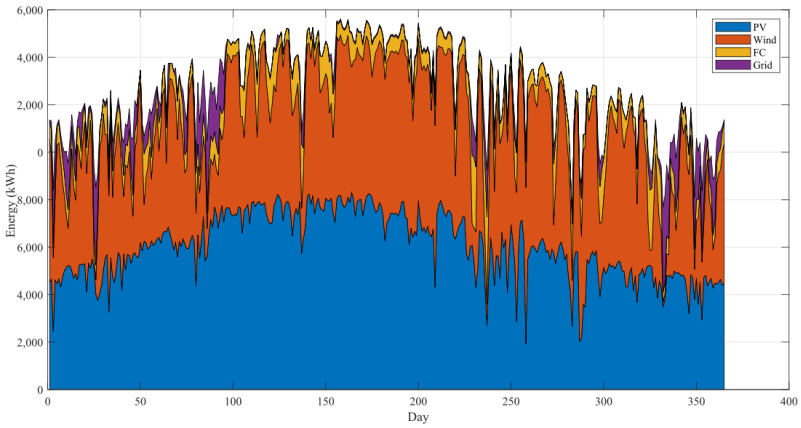

Figure 13. Daily energy supply contributions over a year.

Figure 14 illustrates the hourly operation of the proposed hybrid PV–WT–FC system during the first week of January. **Figure 14a** presents the comparison between total renewable generation (PV + WT), fuel cell output, and load demand, showing that renewable sources supply the majority of the energy, while the fuel cell is activated during deficit periods to ensure continuous power supply. **Figure 14b** depicts the grid interaction, highlighting alternating periods of electricity import and export depending on the balance between generation and demand.

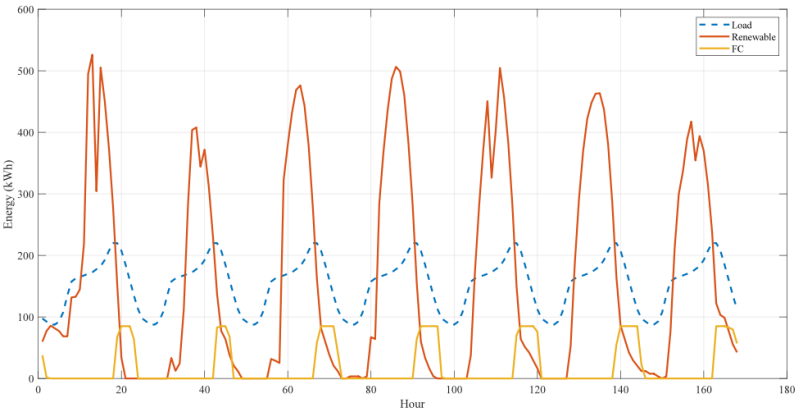

(a)

Figure 14. *Cont.*

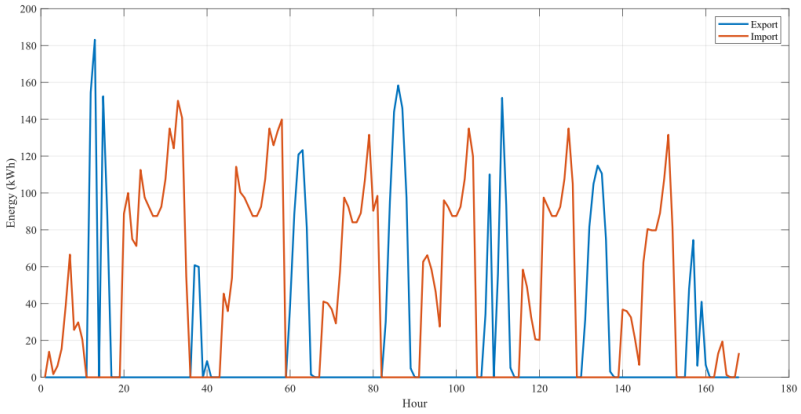

(b)

Figure 14. Hybrid PV–WT–FC performance during the first week of the year: **(a)** Renewable energy weekly production and FC output vs. load; **(b)** Weekly grid exchange.

To further evaluate the dynamic performance of the proposed hybrid PV–WT–FC system, representative weeks from different seasons (January and June) are analyzed, as illustrated in **Figure 15**. **Figure 15** provides a detailed insight into the short-term operational behavior of the system under varying climatic conditions and load patterns.

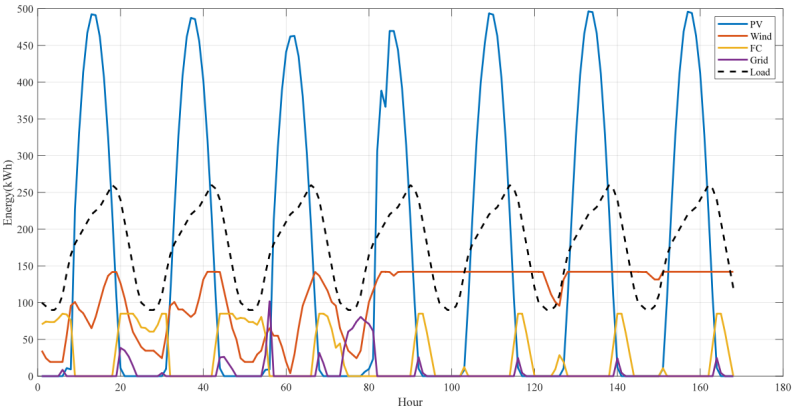

(a)

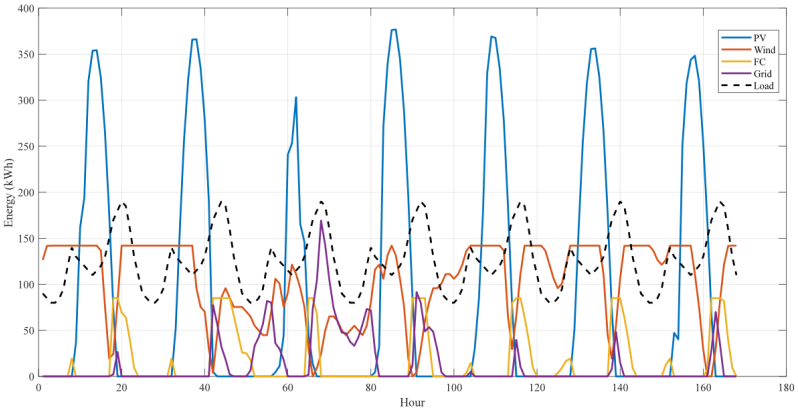

(b)

Figure 15. Hybrid PV–WT–FC performance during the first week of: **(a)** System evolution—January week; **(b)** System evolution—June week.

In January (**Figure 15a**), the system operates under moderate solar availability and variable wind conditions. The PV generation follows the expected daily cycle

but with lower peak values compared to summer months, while wind contributes intermittently. As a result, the system experiences several periods where renewable generation alone is insufficient to meet the load demand. During these intervals, the fuel cell is actively engaged, supported by occasional grid imports, ensuring continuous load satisfaction. This highlights the importance of hydrogen storage and grid support during low renewable availability periods.

In June (**Figure 15b**), the system exhibits significantly improved performance due to higher solar irradiance and relatively stable wind conditions. PV generation reaches its highest levels, often exceeding the load demand during daytime hours. Consequently, the reliance on the fuel cell and grid import is considerably reduced. Instead, surplus energy is either stored or exported, demonstrating enhanced system autonomy and improved renewable energy utilization. This period represents near-optimal operating conditions for the hybrid system.

3.6. Analysis and discussion of system performance during peak load conditions

Figure 16 examines the system's response during a 48-h peak demand interval (starting at 3,625 h). The plot captures the load profile alongside the contributions of PV, wind turbine (WT), fuel cell (FC), and grid exchange, revealing how the components coordinate to maintain power balance.

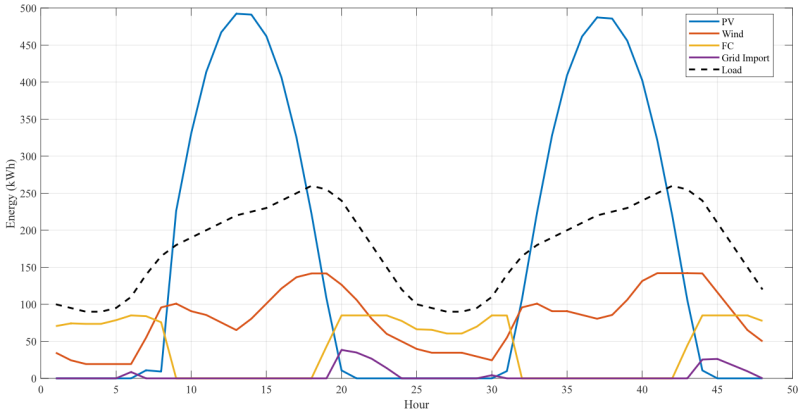

Figure 16. System performance of the PV–WT–FC hybrid system under peak load conditions (48-h peak load period, starting at 3,625 h).

At the beginning of the interval (0–10 h), the load is high while PV output is negligible (nighttime) and wind generation is limited or fluctuating. To cover the deficit, the fuel cell is activated, and the grid may also provide support, demonstrating the system's immediate response to renewable shortages. As solar irradiance increases (10–20 h), PV generation rises, and with possible wind contribution, the reliance on the fuel cell gradually decreases, minimizing grid usage.

During the peak renewable production phase (20–30 h), PV and wind together largely or fully meet the load; the fuel cell operates at a minimum or is turned off, and any excess energy is diverted to hydrogen production, illustrating effective energy storage. When solar radiation declines (30–40 h), PV output drops while wind remains variable, creating a new gap that is compensated by reactivating the fuel cell and, if

needed, by grid support. In the final hours (40–48 h), with PV again negligible and wind possibly insufficient, the fuel cell acts as the primary backup, and the grid serves as a final safety net.

Overall, **Figure 16** confirms that the hybrid system can reliably supply the load during peak demand intervals. PV and wind serve as primary sources whenever available; the fuel cell (backed by hydrogen storage) bridges periods of renewable deficit, and the grid provides a last-resort reliability layer. This coordinated operation ensures uninterrupted power delivery, validating the system's effectiveness under the most challenging conditions.

Figure 17 illustrates the operation of the hybrid system and the behavior of the hydrogen subsystem during the same period of peak load.

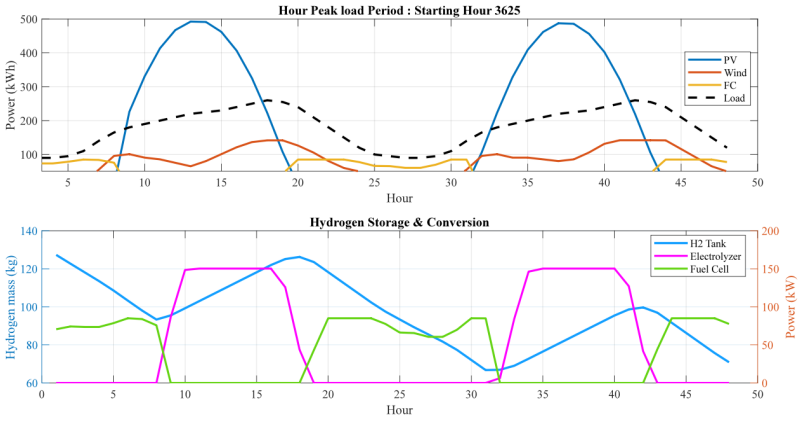

Figure 17. System operation and behavior of the hydrogen subsystem during peak load conditions.

During the analyzed peak load period, the hydrogen subsystem comprising the electrolyzer, hydrogen storage tank, and fuel cell plays a critical role in maintaining the balance between energy supply and demand.

At the beginning of the period, when renewable generation from PV and wind is insufficient, the system experiences a power deficit. In this situation, the fuel cell is activated, converting the stored hydrogen into electrical energy to support the load. The hydrogen tank, therefore, acts as an energy reserve, discharging its stored energy to ensure continuity of supply. If the deficit exceeds the fuel cell capacity, the grid provides additional support.

As renewable generation increases during daylight hours, particularly with rising PV output, the dependence on the fuel cell decreases. When the combined renewable power becomes sufficient to meet the load demand, the fuel cell is either partially loaded or completely turned off. Under these conditions, if excess renewable energy is available, the electrolyzer is activated, converting the surplus electrical energy into hydrogen. This hydrogen is then stored in the tank for later use, effectively shifting energy from periods of surplus to periods of deficit.

During peak renewable generation intervals, the electrolyzer operates at higher capacity, increasing the hydrogen storage level. This process enhances the system's ability to handle future shortages. The hydrogen tank is thus continuously updated, storing energy when excess is available and releasing it when required.

As solar generation declines later in the period and renewable output becomes insufficient again, the system re-enters a deficit state. The electrolyzer is deactivated, and the fuel cell resumes operation, supplying power by utilizing the previously stored hydrogen. This transition highlights the bidirectional role of the hydrogen subsystem as both an energy storage and energy supply mechanism.

Toward the end of the period, when PV generation is negligible and wind power remains limited, the fuel cell becomes the primary internal source of energy. The hydrogen tank continues to discharge until its minimum limit is reached, after which the grid compensates for any remaining unmet demand.

3.7. Discussions validation with existing literature in Morocco, including FC

To validate the effectiveness of the proposed optimization framework, a comparison with existing studies conducted in Morocco involving fuel cell-based hybrid systems is presented in **Table 5**. The results demonstrate that the proposed grid-connected PV–WT–FC system achieves a competitive LCOE of 0.1472 $/kWh, which is significantly lower than several reported configurations, such as PV–WT–FC systems in Dakhla (0.3115 $/kWh [36]) and PV–WT–FC–GES systems in Safi (0.23 €/kWh [37]), while remaining comparable to advanced grid-connected systems in Tangier (0.21 $/kWh [38]). In addition, the proposed system ensures excellent reliability performance (LPSP = 0%) and a high renewable energy fraction (REF = 88.32%), outperforming many previous studies where reliability constraints or renewable penetration were not fully optimized.

Table 5. Similar recent case studies.

System components	Off-Grid (OG)/Grid-Connected (GC)	Location/Application	Economics obtained using various methods	Reliability and others obtained using various methods	Ref.
PV–WT–FC	(Off-Grid/Standalone)	Dakhla City, Morocco Application: Powering a remote, isolated area	LCOE: $0.3115/kWh	LPSP of 0.04647, well within the 5% constraint, indicating high system reliability.	Bouaouda and Sayouti [36]
PV–WT–FC–GES	(Off-Grid/Standalone	Safi, Morocco—Coal plant replacement	LCOE = 0.23 €/kWh at full reliability	100% supply reliability Environmental:	Sahab et al. [37]
PV–WT–BT–FC	Grid connected	Tangier, Morocco—Residential building	LCOE = 0.21 $/kWh	CO_2 reduction of 18.21, 15.13 tCO_2e/year	Elaouzy et al. [38]
WT–FC–DG–FC	(Off-Grid/Standalone	Dakhla, Morocco/Remote off-grid residential settlement	LCOE: $0.0701/kWh	44.57% renewable fraction;	El Hassani et al. [39]
PV–WT–FC	Grid connected	Dakhla City, Morocco Application: Powering an isolated area	LCOE = 0.1472	LPSP = 0% REF = 88.32% Dgs = 0.33 Dload = 0.988	This work

Although the WT–FC–DG–FC configuration reported in El Hassani et al.'s study [39] achieves the lowest LCOE (0.0701 $/kWh), this result is obtained at the expense of a relatively low renewable energy fraction (44.57%). This indicates a significant dependence on non-renewable sources, with more than half of the energy supplied by conventional generation. Consequently, despite its economic advantage, such a configuration cannot be considered fully sustainable from an environmental perspective. In contrast, the proposed system achieves a more balanced trade-off by combining competitive cost with a high renewable energy penetration, thereby ensuring both economic viability and environmental sustainability.

The superior performance observed in this study is a direct consequence of the adopted optimization methodology. By integrating economic, reliability, and grid stability constraints within a unified framework, the proposed approach enables the identification of system configurations that are not only cost-effective but also operationally stable and environmentally sustainable. This comprehensive formulation explains the improved results achieved, particularly the combination of low LCOE, zero loss of power supply probability (LPSP), and high renewable energy fraction (REF). In addition to its competitive economic performance, the proposed system demonstrates enhanced reliability and high renewable energy penetration, reflecting a well-balanced trade-off between cost efficiency and operational performance. These outcomes clearly highlight the effectiveness of the multi-constraint optimization approach, which ensures more robust and realistic solutions compared to previous studies in the same region, where optimization is often limited to individual study aspects rather than a comprehensive multi-criteria evaluation.

4. Conclusions

This study investigated the techno-economic and environmental performance of grid-connected hybrid renewable energy systems (HRES) for a case study in Dakhla, Morocco. Three system configurations, PV–WT–FC, WT–FC, and PV–FC, were analyzed by optimizing the capacities of photovoltaic panels, wind turbines, electrolyzers, hydrogen storage tanks, and fuel cells under an advanced energy management strategy.

A comprehensive system-level modeling framework was developed, integrating detailed mathematical representations of all system components and their interactions. The optimization problem was formulated to minimize the total annual cost while incorporating penalty terms related to system reliability and grid stability. Key performance indicators, including the levelized cost of energy (LCOE), renewable energy fraction (REF), loss of power supply probability (LPSP), and grid fluctuation indices, were evaluated to ensure a multi-dimensional assessment of system performance.

The results demonstrated that the PV–WT–FC configuration represents the most optimal solution, achieving a total annual cost of 186,957 USD and an LCOE of 0.1472 USD/kWh, along with a high renewable energy fraction of 88.32%. This configuration also ensured excellent reliability (LPSP = 0.0000) and stable grid operation. In contrast, although the WT–FC configuration yielded a lower LCOE when considering only

component costs, it exhibited significant grid instability, leading to high penalty costs and reduced overall feasibility. Similarly, the PV–FC configuration showed higher costs and lower renewable penetration, making it less competitive.

These findings highlight a key contribution of this work: the necessity of integrating grid stability constraints and penalty mechanisms into the optimization framework. Relying solely on economic indicators such as LCOE can lead to suboptimal or impractical system configurations; therefore, a holistic evaluation that includes economic, environmental, reliability, and grid stability aspects is essential for accurate system design.

Overall, the PV–WT–FC system provides the best trade-off among all considered criteria, offering a balanced solution in terms of cost, reliability, environmental performance, and operational stability. The integration of hydrogen storage plays a crucial role in enhancing system flexibility by enabling efficient energy storage and mitigating renewable intermittency, thereby reducing dependence on the grid.

The findings of this study have important practical implications for the design and deployment of hybrid renewable energy systems, particularly in regions with high renewable potential such as Morocco. The proposed framework can support decision-makers in selecting optimal system configurations that balance multiple performance objectives while ensuring system feasibility under real operating conditions. Furthermore, the results provide useful guidelines for component sizing and energy management in grid-connected hybrid systems.

Future research should focus on extending the proposed framework by incorporating more advanced component models that account for part-load behavior, temperature effects, and degradation mechanisms. In addition, the development of intelligent energy management strategies based on predictive or artificial intelligence techniques, as well as the comparison of different optimization algorithms, could further enhance system performance. Finally, experimental validation and pilot-scale implementation are recommended to assess the real-world applicability of the proposed approach.

Author contributions: Conceptualization, methodology, software, formal analysis, investigation, resources, data curation, writing—original draft preparation, and visualization, YEB; supervision, project administration, writing—review and editing, and funding acquisition, MF; writing—review and editing, MF and SK; validation, YEB, MF and SK. All authors have read and agreed to the published version of the manuscript.

Funding: This work received no external funding.

Institutional review board statement: Not applicable.

Informed consent statement: Not applicable.

Data availability statement: Data will be made available on request.

Conflict of interest: The authors declare no conflict of interest.

AI use statement: During the preparation of this manuscript, the authors used AI solely

for language refinement. No AI tools were used for data analysis, interpretation, or generation of scientific content. All outputs were critically reviewed and edited by the authors. The authors take full responsibility for the integrity and accuracy of the work.

Abbreviations

Symbol	Description	Unit
P_{PV}	Instantaneous photovoltaic power output	kW
E_{PV}	Total photovoltaic energy output	kWh
P_{WT}	Wind turbine power output	kW
E_{WT}	Wind energy production	kWh
$P_{FC\text{-}inv}$	Fuel cell electrical output	kW
$P_{Elz\text{-}H_{2\_tank}}$	Power transferred from electrolyzer to hydrogen tank	kW
$P_{H_{2\_tank}\text{-}FC}$	Power supplied from hydrogen tank to fuel cell	kW
P_{ren}	Total renewable power (PV + WT)	kW
P_{load}	Load demand	kW
$P_{deficit}$	Power deficit	kW
P_{surp}	Surplus power	kW
$P_{inv\text{-}load}$	Power supplied to load after inverter	kW
E_{total}	Total generated energy	kWh
$E_{H_{2\_tank}}$	Energy stored in hydrogen tank	kWh
$E_{H_{2\_tank\_max}}$	Maximum hydrogen storage capacity	kWh
m_{H_2}	Hydrogen mass stored	kg
$m_{H_{2,c}}$	Hydrogen consumption	kg
HHV_{H_2}	Higher heating value of hydrogen	kWh/kg
$P_{H_{2\_produced}}$	Hydrogen production rate	kW
η_{PV}	Photovoltaic efficiency	–
η_{Elz}	Electrolyzer efficiency	–
η_{FC}	Fuel cell efficiency	–
η_{HST}	Hydrogen storage efficiency	–
μ_{inv}	Inverter efficiency	–
β	PV temperature coefficient	1/°C
NOCT	Nominal operating cell temperature	°C
G	Solar irradiance	W/m^2
G_{ref}	Reference irradiance	W/m^2
T	Cell temperature	°C
T_{amb}	Ambient temperature	°C
W_h	Wind speed at hub height	m/s
W_{ref}	Wind speed at reference height	m/s
H_h	Hub height	m
H_{ref}	Reference height	m
n	Wind shear exponent	–
P_{rated}	Rated wind turbine power	kW
W_{Ci}	Cut-in wind speed	m/s
W_r	Rated wind speed	m/s

W_{Co}	Cut-off wind speed	m/s
X	Decision vector of optimization variables	–
N_{PV}	Number of PV units	–
N_{WT}	Number of wind turbines	–
N_{FC}	Number of electrolyzers	–
N_{Elz}	Number of hydrogen tanks	–
N_{Tank}	Number of fuel cells	–
TAC	Total annual cost	$
LCOE	Levelized cost of energy	$/kWh
$C_{capital}$	Capital cost	$
$C_{O\&M}$	Operation and maintenance cost	$
$C_{replacement}$	Replacement cost	$
$C_{salvage}$	Salvage value	$
$C_{grid,imp}$	Cost of imported electricity	$
$C_{grid,exp}$	Revenue from exported electricity	$
λ_{imp}	Electricity import tariff	$/kWh
λ_{exp}	Electricity export tariff	$/kWh
CRF	Capital recovery factor	–
r	Discount rate	–
F_{HREs}	System lifetime	years
LPSP	Loss of Power Supply Probability	–
REF	Renewable energy fraction	–
F_{grid}	Load fluctuation index	–
D_{load}	Grid fluctuation index	–
β_L	Maximum allowable LPSP	–
β_g	Grid fluctuation limit	–
t_{CO_2}	CO_2 emissions avoided	t/year
EF	Emission factor	t/kWh
t	Time step	h
Δt	Time interval	h
N	Number of time steps (8,760)	–

References

1. Sohaib M, Majeed A, Liu J, et al. The role of renewable energy in mitigating carbon emissions: Insights from China's energy consumption patterns. Energy Strategy Reviews. 2025; 61: 101860. doi: 10.1016/j.esr.2025.101860
2. Singh S, Slowik A, Kanwar N, et al. Techno-economic feasibility analysis of grid-connected microgrid design by using a modified multi-strategy fusion artificial bee colony algorithm. Energies. 2021; 14(1): 190. doi: 10.3390/en14010190
3. Bade SO, Tomomewo OS, Meenakshisundaram A, et al. Multi-Criteria Optimization of a Hybrid Renewable Energy System Using Particle Swarm Optimization for Optimal Sizing and Performance Evaluation. Clean Technologies. 2025; 7(1): 23. doi: 10.3390/cleantechnol7010023
4. Iqbal MN, Bhatti AR, Farhan M, et al. Optimizing the design of hybrid renewable energy systems considering electric vehicle loading. Electric Power Systems Research. 2026; 252: 112452. doi: 10.1016/j.epsr.2025.112452
5. Taghavi M, Lee CJ. Development of a novel hydrogen liquefaction structure based on liquefied natural gas regasification operations and solid oxide fuel cell: Exergy and economic analyses. Fuel. 2025; 384: 133826. doi:

10.1016/j.fuel.2024.133826
6. Falope T, Lao L, Hanak D, et al. Hybrid energy system integration and management for solar energy: A review. Energy Conversion and Management: X. 2024; 21: 100527. doi: 10.1016/j.ecmx.2024.100527
7. Alharbi AM, Ali ZM, Diab AAZ. Comparative techno-economic optimization of microgrid configurations using hybrid battery–hydrogen storage: NEOM case study, Saudi Arabia. 2025; 20(9): e0326050. doi: 10.1371/journal.pone.0326050
8. Duan F, Eslami M, Okati M, et al. Hybrid stochastic and robust optimization of a hybrid system with fuel cell for building electrification using an improved arithmetic optimization algorithm. Scientific Reports. 2025; 15(1): 1779. doi: 10.1038/s41598-025-86074-z
9. Taghavi M, Yoon HJ, Choi JU, et al. Innovative Structure of a Liquefied Natural Gas (LNG) Process by Mixed Fluid Cascade Using Solar Renewable Energy, Photovoltaic Panels (PV), and Absorption Refrigeration System. In: Manenti F, Reklaitis GV (editors). Computer Aided Chemical Engineering. Elsevier; 2024. 53, pp. 2071–2076. doi: 10.1016/B978-0-443-28824-1.50346-X
10. Taghavi M, Lee CJ. Development of novel hydrogen liquefaction structures based on waste heat recovery in diffusion-absorption refrigeration and power generation units. Energy Conversion and Management. 2024; 302: 118056. doi: 10.1016/j.enconman.2023.118056
11. Agoundedemba M, Kim CK, Kim HG, et al. Modelling and optimization of microgrid with combined genetic algorithm and model predictive control of PV/Wind/FC/battery energy systems. Energy Reports. 2025; 13: 238–255. doi: 10.1016/j.egyr.2024.12.008
12. Liao W, Xiong Q, Chen Z, et al. Stochastic sizing and energy management of a hybrid energy system using cloud model and improved Walrus optimizer for China regions. Scientific Reports. 2025; 15(1): 21205. doi: 10.1038/s41598-025-03212-3
13. Al-Shetwi AQ. Feasibility study on optimal hybrid renewable energy systems in northern Saudi Arabia: Technical, economic, and environmental assessments. International Journal of Ambient Energy. 2025; 46(1): 2540583. doi: 10.1080/01430750.2025.2540583
14. Duan F, Basem A, Sawaran Singh NS. Stochastic designing of a hybrid system with hydrogen energy management based-fuel cell using machine learning and improved arithmetic optimization algorithm for building electrification. Energy. 2025; 334: 137509. doi: 10.1016/j.energy.2025.137509
15. Sultan HM, Menesy AS, Kamel S, et al. An improved artificial ecosystem optimization algorithm for optimal configuration of a hybrid PV/WT/FC energy system. Alexandria Engineering Journal. 2021; 60(1): 1001–1025. doi: 10.1016/j.aej.2020.10.025
16. Yasmin R, Nabi MN, Rashid F, et al. Solar, Wind, Hydrogen, and Bioenergy-Based Hybrid System for Off-Grid Remote Locations: Techno-Economic and Environmental Analysis. Clean Technologies. 2025; 7(2): 36.
17. Coban HH. A multiscale approach to optimize off-grid hybrid renewable energy systems for sustainable rural electrification: Economic evaluation and design. Energy Strategy Reviews. 2024; 55: 101527. doi: 10.1016/j.esr.2024.101527
18. Drici M, Houabes M, Salawudeen AT, et al. Optimizing Hybrid Renewable Energy Systems for Isolated Applications: A Modified Smell Agent Approach. Eng. 2025; 6(6): 120. doi: 10.3390/eng6060120
19. Alharthi YZ. An Analysis of Hybrid Renewable Energy-Based Hydrogen Production and Power Supply for Off-Grid Systems. Processes. 2024; 12(6): 1201. doi: 10.3390/pr12061201
20. Serat Z, Danishmal M, Mohammad Mohammadi F. Optimizing hybrid PV/Wind and grid systems for sustainable energy solutions at the university campus: Economic, environmental, and sensitivity analysis. Energy Conversion and Management: X. 2024; 24: 100691. doi: 10.1016/j.ecmx.2024.100691
21. Azam ME, Anika ST, Ali MF, et al. Evaluating Renewable–Hydrogen Hybrid Microgrids for Remote Island Electrification in Bangladesh. In: Proceedings of the 2026 5th International Conference on Electrical, Computer & Telecommunication Engineering (ICECTE); 29–31 January 2026; Rajshahi, Bangladesh. pp. 1–6. doi: 10.1109/ICECTE69292.2026.11429221
22. Ermiş S, Taşdemir O, Al-Hajj R. Multi-objective techno-economic and environmental optimization of hydrogen-based hybrid renewable energy system using osprey optimization algorithm. Scientific Reports. 2026. doi: 10.1038/s41598-026-45185-x
23. Abdoulaye MA, Waita S, Wekesa C.W, et al. Multi-criteria optimal sizing and analysis of PV/wind/fuel cell/battery/diesel generator for rural electrification: A case study in Chad. International Journal of Renewable Energy Development. 2024; 13(3): 491–507. doi: 10.61435/ijred.2024.60169

24. Turcios LJ, Torres-Madroñero JL, Cárdenas LM, et al. Assessment of Hybrid Renewable Energy System: A Particle Swarm Optimization Approach to Power Demand Profile and Generation Management. Energies. 2025; 18(23): 6141. doi: 10.3390/en18236141
25. Mohapatra S, Kaliyaperumal D, Porselvi T, et al. Optimal sizing of hybrid renewable energy systems relying on the black winged kite algorithm for performance evaluation. Scientific Reports. 2025; 15(1): 20568. doi: 10.1038/s41598-025-06442-7
26. González Cusa Y, Hidalgo Suárez J, Moya Rodríguez JL, et al. Optimal Sizing of an Off-Grid Hybrid Energy System with Metaheuristics and Meteorological Forecasting Based on Wavelet Transform and Long Short-Term Memory Networks. Energies. 2025; 18(20): 5371. doi: 10.3390/en18205371
27. AL Dawsari SA, Anayi F, Packianather M. Optimizing a hybrid off-grid photovoltaic/wind/fuel cell energy system using mantis search algorithm. Energy Conversion and Management: X. 2025; 27: 101209. doi: 10.1016/j.ecmx.2025.101209
28. Bade SO, Tomomewo OS. Optimizing a hybrid wind-solar-biomass system with battery and hydrogen storage using generic algorithm-particle swarm optimization for performance assessment. Cleaner Energy Systems. 2024; 9: 100157. doi: 10.1016/j.cles.2024.100157
29. El-Sattar HA, Kamel S, Sultan HM, et al. Optimal design of Photovoltaic, Biomass, Fuel Cell, Hydrogen Tank units and Electrolyzer hybrid system for a remote area in Egypt. Energy Reports. 2022; 8: 9506–9527. doi: 10.1016/j.egyr.2022.07.060
30. Güven AF, Yörükeren N, Tag-Eldin E, et al. Multi-Objective Optimization of an Islanded Green Energy System Utilizing Sophisticated Hybrid Metaheuristic Approach. IEEE Access. 2023; 11: 103044–103068. doi: 10.1109/ACCESS.2023.3296589
31. Wang Y, He X, Liu Q, et al. Economic and technical analysis of an HRES (Hybrid Renewable Energy System) comprising wind, PV, and fuel cells using an improved subtraction-average-based optimizer. Heliyon. 2024; 10(12): e32712. doi: 10.1016/j.heliyon.2024.e32712
32. Mohamed MA, Shadoul M, Yousef H, et al. Multi-agent based optimal sizing of hybrid renewable energy systems and their significance in sustainable energy development. Energy Reports. 2024; 12: 4830–4853. doi: 10.1016/j.egyr.2024.10.051
33. Xu L, Ruan X, Mao C, et al. An Improved Optimal Sizing Method for Wind-Solar-Battery Hybrid Power System. IEEE Transactions on Sustainable Energy. 2013; 4(3): 774–785. doi: 10.1109/TSTE.2012.2228509
34. Güven AF, Yörükeren N. A comparative study on hybrid GA-PSO performance for stand-alone hybrid energy systems optimization. Sigma Journal of Engineering and Natural Sciences. 2024; 42(5): 1410–1438.
35. Singh A, Sharma A, Rajput S, et al. An Investigation on Hybrid Particle Swarm Optimization Algorithms for Parameter Optimization of PV Cells. Electronics. 2022; 11(6): 909. doi: 10.3390/electronics11060909
36. Bouaouda A, Sayouti Y. Design optimization of a multi-source renewable energy system using a novel method based on selective ensemble learning. Procedia Computer Science. 2024; 236: 111–118. doi: 10.1016/j.procs.2024.05.011
37. Sahab M, Emrani A, Sanjari MJ, et al. Optimal design and energy management of a hybrid PV-Wind system with hydrogen and gravity energy storage: An off-grid sustainable alternative for coal power in Morocco. Renewable Energy Focus. 2026; 56: 100775. doi: 10.1016/j.ref.2025.100775
38. Elaouzy Y, El Fadar A, Achkari OB. Assessing the 3E performance of multiple energy supply scenarios based on photovoltaic, wind turbine, battery and hydrogen systems. Journal of Energy Storage. 2024; 99: 113378. doi: 10.1016/j.est.2024.113378
39. El Hassani S, Oueslati F, Horma O, et al. Techno-economic feasibility and performance analysis of an islanded hybrid renewable energy system with hydrogen storage in Morocco. Journal of Energy Storage. 2023; 68: 107853. doi: 10.1016/j.est.2023.107853